ResearchGate

See discussions, stats, and author profiles for this publication at: https://www.researchgate.net/publication/350621564

Comprehensive Characterisation of the Morphological, Thermal and Kinetic Degradation Properties of Gluconacetobacterxylinus synthesised Bacterial Nanocellulose

Article *in* Journal of Natural Fibers · April 2021

DOI: 10.1080/15440478.2021.1907833

CITATIONS
2

READS
74

8 authors, including:

Bemgba B. Nyakuma
UTM Centre for Low Carbon Transport in Cooperation with Imperial College (UTM …
199 PUBLICATIONS **1,127** CITATIONS
SEE PROFILE

Wong Syie Luing
King Juan Carlos University
93 PUBLICATIONS **2,306** CITATIONS
SEE PROFILE

Laura Nguoron Utume
Benue State University, Makurdi
14 PUBLICATIONS **21** CITATIONS
SEE PROFILE

Tuan Amran Tuan Abdullah
Universiti Teknologi Malaysia
193 PUBLICATIONS **2,740** CITATIONS
SEE PROFILE

Some of the authors of this publication are also working on these related projects:

Gasification of Biomass to syngas View project

Biohydrogen Production View project

All content following this page was uploaded by Bemgba B. Nyakuma on 04 April 2021.

The user has requested enhancement of the downloaded file.

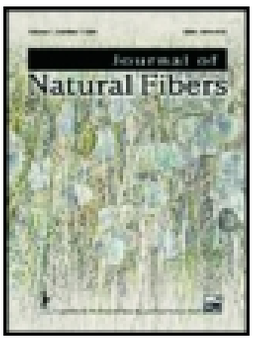

Journal of Natural Fibers

ISSN: (Print) (Online) Journal homepage: https://www.tandfonline.com/loi/wjnf20

Comprehensive Characterisation of the Morphological, Thermal and Kinetic Degradation Properties of *Gluconacetobacter xylinus* synthesised Bacterial Nanocellulose

Bemgba B. Nyakuma, Syieluing Wong, Laura N. Utume, Tuan Amran T. Abdullah, Mustapha Abba, Olagoke Oladokun, Tertsegha J-P. Ivase & Ezekiel B. Ogunbode

To cite this article: Bemgba B. Nyakuma, Syieluing Wong, Laura N. Utume, Tuan Amran T. Abdullah, Mustapha Abba, Olagoke Oladokun, Tertsegha J-P. Ivase & Ezekiel B. Ogunbode (2021): Comprehensive Characterisation of the Morphological, Thermal and Kinetic Degradation Properties of *Gluconacetobacter xylinus* synthesised Bacterial Nanocellulose, Journal of Natural Fibers, DOI: 10.1080/15440478.2021.1907833

To link to this article: https://doi.org/10.1080/15440478.2021.1907833

Published online: 04 Apr 2021.

Submit your article to this journal

View related articles

View Crossmark data

Full Terms & Conditions of access and use can be found at
https://www.tandfonline.com/action/journalInformation?journalCode=wjnf20

JOURNAL OF NATURAL FIBERS
https://doi.org/10.1080/15440478.2021.1907833

Taylor & Francis
Taylor & Francis Group

ARTICLE

Check for updates

Comprehensive Characterisation of the Morphological, Thermal and Kinetic Degradation Properties of *Gluconacetobacter xylinus* synthesised Bacterial Nanocellulose

Bemgba B. Nyakuma[a], Syieluing Wong[b], Laura N. Utume[c], Tuan Amran T. Abdullah[d], Mustapha Abba[e], Olagoke Oladokun[f], Tertsegha J-P. Ivase[g], and Ezekiel B. Ogunbode[h]

[a]Research Initiative for Sustainable Energy Technologies (RISET), Makurdi, Benue State, Nigeria; [b]Departamento Matemática Aplicada, Ciencia E Ingeniería De Materiales Y Tecnología Electrónica, Universidad Rey Juan Carlos, Madrid, Spain; [c]Department of Biological Sciences, Faculty of Sciences, Benue State University, Makurdi, Benue State, Nigeria; [d]School of Chemical and Energy Engineering, Faculty of Engineering, Universiti Teknologi Malaysia, Skudai, Johor, Malaysia; [e]Department of Microbiology, Faculty of Science, Bauchi Statem, University, Gadau, Bauchi State, Nigeria; [f]Department of Chemical Engineering, College of Engineering, Covenant University, Ota, Ogun State, Nigeria; [g]Bio-Resource Development Centre, National Biotechnology Development Agency, Makurdi, Benue State, Nigeria; [h]Department of Building, Federal University of Technology Minna (FUT Minna), Niger State, Nigeria

ABSTRACT

Microbial-assisted synthesis can advance nanocellulose production, while addressing the economics and environmental friendliness of conventional techniques. Bacterial nanocellulose (BNC) is a linear exopolysaccharide with 3-D structures and nanofibril networks synthesized by various bacteria. The physical, chemical and mechanical properties of BNC have been characterized for various applications. However, limited knowledge of the thermal degradation and kinetic properties of BNC currently hampers its utilization as renewable biopolymers as heat, temperature, and heating rates influence life span and future applications. Therefore, this study examines the thermal, chemical, morphological, microstructure, and kinetic properties of *Gluconacetobacter xylinus* synthesized BNC through thermogravimetric analysis (TGA), scanning electron microscopy (SEM), energy dispersive X-ray (EDX), and isoconversional Ozawa–Flynn–Wall (OFW) kinetic modeling. The SEM results showed that BNC has a highly dense fibril structure with overlapping knots, which denotes a high surface area, porosity and crystallinity, whereas EDX revealed C, O, and Na. TGA revealed BNC undergoes three-stage thermal degradation with mass loss of 53.57% and residual mass of 46.43% on average. Kinetic modeling revealed the average activation energy (E_a = 59.39 kJ/mol) and pre-exponential factor (k_o = 1.62 × 10^{10} min^{-1}) for BNC indicating high thermal reactivity. Thus, *G. xylinus*- synthesized BNC has potential for many applications in the future.

摘要

微生物辅助合成可以促进纳米纤维素的生产，同时解决传统技术的经济性和环境友好性. 细菌纳米纤维素（BNC）是由多种细菌合成的具有三维结构和纳米纤维网络的线性胞外多糖. BNC的物理、化学和机械性能已在各种应用中得到表征. 然而, 有限的知识热降解和动力学性质的BNC目前阻碍了其作为可再生生物聚合物的利用, 因为热量, 温度和加热率影响寿命和未来的应用. 因此, 本研究通过热重分析（TGA）、扫描电子显微镜（SEM）、能量色散X射线（EDX）和等转化率Ozawa-Flynn-Wall（OFW）动力学模型研究了葡萄糖酸杆菌合成BNC的热、化学、形态、微观结构和动力学性质. 扫描电镜（SEM）结果表明，BNC具有高度致密的纤维结构

KEYWORDS
Thermogravimetry; kinetics; bacterial nanocellulose; *Gluconacetobacter xylinus*

关键词
热重分析法; 动力学; 细菌纳米纤维素; 木葡糖酸杆菌

CONTACT Bemgba B. Nyakuma bbnyax1@gmail.com Research Initiative for Sustainable Energy Technologies (RISET), Makurdi, Nigeria.

© 2021 Taylor & Francis

和重叠的节, 这表明BNC具有较高的比表面积、孔隙率和结晶度, 而EDX显示C、O和Na. TGA分析表明, BNC经历了三个阶段的热降解FF0C质量损失为53.57%, 平均残余质量为46.43%. 动力学模型显示BNC的平均活化能（Ea=59.39kJ/mol）和指数前因子（ko=1.62×1010min-1）表明其具有较高的热反应活性. 因此, 木霉合成的BNC具有广阔的应用前景.

Introduction

The isolation and synthesis of nanocelluloses (NC) have gained significant attention over the years due to their unique material properties (Kargarzadeh et al. 2012). The NC materials derived from renewable and sustainable sources are abundant, low cost, biodegradable, and environmentally friendly (Jozala et al. 2016; Shah et al. 2013a; Shankar and Rhim 2016). However, current techniques such as acid hydrolysis (Peretz et al., 2019), electrospinning (Han et al., 2019), irradiation (Kim et al., 2016), mechanical grinding (Zhuo et al. 2017), and combined ozonation with hydrolysis (Peretz et al., 2019) utilized for isolating and synthesizing NCs are hazardous, expensive, and time-consuming (Kalia et al., 2011; Reddy and Rhim, 2014). Furthermore, the isolation or synthesis of NCs from agricultural waste is characterized by low yields and process efficiencies along with high product impurities due to the presence of lignin and other polysaccharides found in plants (Li et al. 2018; Phanthong et al. 2016). Hence, the NCs require additional treatments or purifications to obtain pure variants for specialized applications in the pharmaceutical and biomedical industries. Scientists have examined the synthesis of NCs from microbial species such as bacteria to address these challenges (Fu et al. 2013b; Jozala et al. 2016). Numerous studies have isolated and synthesized bacterial nanocellulose (BNC) from various bacteria genera such as *Rhizobium leguminosarum* (Mohammadkazemi et al. 2015), *Gluconacetobacter xylinus* (Jozala et al. 2016), *Pseudomonas putida*, and *Salmonella enterica* (Blanco et al. 2018), *Komagataeibacter* (Skočaj 2019), *Agrobacterium tumefaciens, Dickeya dadantii* and *Escherichia coli* (Jacek et al. 2019) among others reported in the literature.

BNC is a linear exopolysaccharide comprising β-D-glucopyranose monomer components connected by β-1,4-glycosidic chains (Jacek et al. 2019; Martínez Ávila et al. 2014). BNC contains 99% moisture in its natural state, which makes it a hydrogel with interesting materials applications (Klemm et al. 2001). The structure of BNC consists of a 3-D network is comprised of nanofibrils that range from 70 to 140 nm wide, which is similar to collagen. It is also characterized by high surface area, which is stabilized by inter- and intra-fibrillar hydrogen bonds (Martínez Ávila et al. 2014). BNC has high mechanical strength, crystallinity, purity, porosity, young modulus, water-binding capacity, tensile strength properties along with high surface area, low density and oxygen permeability (Blanco et al. 2018; Martínez Ávila et al. 2014; Zhuo et al. 2017), which are critical to the production of biopolymers for various applications. The excellent mechanical properties of BNC are responsible for its application as a reinforcing agent for drug delivery, scaffolds regeneration, skin transplants, wounds and burn dressings (Fu et al. 2013b; Gatenholm and Klemm 2010). Other notable applications include biotechnology, pharmaceuticals, medicine, bio-based packaging, cosmetics, paper manufacturing, coating and composite materials (Curvello, Raghuwanshi, and Garnier 2019; Kamel et al. 2020; Lin and Dufresne 2014). The ability of bacteria to synthesize BNC as an advanced functional material has future potential far beyond the existing applications reported in the literature.

Previous studies have employed various analytical techniques such as X-ray diffraction (XRD), scanning electron microscopy (SEM), energy dispersive X-ray (EDX), Fourier transform infrared (FTIR) spectroscopy, and thermogravimetric analysis (TGA) to investigate the crystallinity, morphology, bulk chemical composition, functional group chemistry and thermal properties of bio-based materials (Abba et al. 2020; Bhattacharya et al. 2020; Derami et al. 2019; Nyakuma et al. 2020b). The previous study by Abba et al. (2017) isolated BNC from *G. xylinus* and characterized its material properties through FTIR, XRD, SEM, and EDX. However, there are limited studies on the thermal

degradation behavior and kinetic decomposition mechanism of BNC in the literature. Since temperature and heating rates play an influential role in the thermal stability, performance, life span, and potential applications of polymeric materials, it is critical to examine the thermal and kinetic properties of BNC. Hence, the present study seeks to investigate the thermal degradation behavior and decomposition kinetics of BNC synthesized from *G. xylinus* under non-isothermal and multiple heating rate-TGA using the isoconversional kinetic model of Ozawa-Flynn-Wall (OFW). The study also presents the morphological, microstructure, and bulk chemical properties of *G. xylinus* synthesized BNC. To the best of the author's knowledge, this is the first comprehensive study on the multiple heating rate thermal, non-isothermal and isoconversional kinetic characterization of *G. xylinus* synthesized bacterial nanocellulose (BNC) in the literature.

Materials and Methods

Materials, Synthesis, and Purification of BNC from *G. xylimus* BCZM

The reagents employed in the synthesis, recovery and purification of BNC from *G. xylinus* were as follows: peptone, citric acid, disodium hydrogen phosphate, glucose, yeast extracts, sodium hydroxide, agar, ethanol and sodium hydroxide, which were all purchased in analytical grade from Bacto, Merck and Sigma–Aldrich (USA). Contamination was avoided through aseptic handling and storage of samples and the media before and after each experiment. The Hestrin and Schramm (HS) broth selected for the synthesis of *G. xylinus* in this study was prepared at pH 5.5 (Hestrin and Schramm 1954). The pre-inoculum was prepared by transporting the pure *G. xylinus* BCZM colonies to the 50 mL HS broth before incubating for 3 days at 30°C with constant stirring at 100 rpm. The energetic agitation of the culture broth was performed to release the cells into the broth. The inoculum was prepared in triplicates using 10% v/v with fresh HS broth in a 250-mL conical flask. The flask was subsequently incubated for 7 days under static conditions at 30°C. The formation of a thick gelatinous layer on the surface of the culture broth confirmed the production of BNC (Jozala et al. 2016; Yang et al. 2013). The BNC pellicles were recovered by simple filtration and cleaned with deionized water to remove extraneous materials and impurities. The BNC was then purified and treated based on the procedures of the alkaline method described by Abba et al. (2017). Lastly, the purified BNC was subjected to oven and freeze-drying to obtain the dried film used for material characterization and further analysis.

Morphological and Bulk Chemical Analyses

The scanning electron microscope (SEM, JOEL JSM-6390 LV, Japan) was employed to examine the morphology and microstructure of the synthesized BNC. The sample surface was prepared for SEM analysis by sputter coating a thin layer of gold (Au) using the automatic sputter coater (Quorum Q150R S, U.K). Sputter coating was done to enhance the conductivity of the sample and the image quality of the SEM micrographs (Trovatti et al., 2011). The sample was then transferred to the sample chamber and degassed before scanning at a magnification of ×30,000 to obtain the SEM micrographs. The SEM microscope was operated under high vacuum at the following conditions; 50 pA, 30 kV (accelerating voltage), and 5 mm (working distance). In contrast, the energy dispersive X-ray (EDX) technique was employed to examine the bulk chemical properties of the BNC sample. The EDX analysis was performed using the point ID and mapping feature of the SEM Microscope to compute the composition of chemical elements (weight percent, wt.%) of BNC from the charge balance.

Thermogravimetric Analysis (TGA)

The thermal degradation behavior and properties of the *G. xylinus* BCZM-synthesized BNC were examined by thermogravimetric analysis (TGA). During each TGA test, approximately 16 ± 0.60 mg

of the BNC sample was placed in an alumina crucible after which the furnace was purged with nitrogen gas (N_2, flow rate 20 mL/min) to ensure an inert environment in the TGA furnace (Shimadzu TG-50, Japan). Next, each sample was heated at the selected heating rate from 10°C/min to 50°C/min (in 10°C/min increments) from 28°C to 700°C based on the selected non-isothermal TGA program. On completion, the raw thermogram data were analyzed using the thermal analysis software (Shimadzu TA-60WS workstation) to acquire the stepwise mass loss (ML) and derivative ML data for each TGA run. Next, the thermogravimetric (TG, %) and derivative thermogravimetric (DTG, %) data were plotted against temperature (°C) in Microsoft Excel.

Temperature Profile Analysis (TPA)

The effects of temperature, heating rates, and reaction time on the thermal degradation behavior and residual product properties after TGA were examined through the temperature profile characteristics (TPC). In this study, the TPCs were deduced from the TG-DTG plots using the data analysis feature of the Shimadzu TA-60WS workstation software, as described in the literature (Nyakuma et al. 2020a; Nyakuma, Wong, and Oladokun 2019). Based on the TG plots, the TPCs, namely; ignition (T_{ons}), midpoint (T_{mid}), peak decomposition (T_{max}), burnout (T_{off}) temperatures along with the mass loss (ML) residual mass (RM) were determined. In contrast, the TPCs, namely drying peaks I and II ($T_{dry,\mathrm{I}}$ and $T_{dry,\mathrm{II}}$), maximum decomposition peak (T_{max}) temperature, and lastly mass-loss rates (MLR I, II) and MLR III for drying and devolatilization were deduced from the DTG plots, respectively.

Kinetic Modeling Analysis (KMA)

The analysis of the kinetic parameters, activation energy (E_a) and pre-exponential factor (k_o) for the thermal degradation of BNC, was computed from the isoconversional kinetic model of Ozawa–Flynn–Wall (OFW). The OFW model is widely employed to examine the kinetic parameters of thermally degrading carbonaceous materials under multiple heating rates, non-isothermal, and non-oxidative conditions (Dwivedi, Karmakar, and Chatterjee 2020; Soria-Verdugo et al. 2018). The governing equations of the OFW model presented in Equation 1 are derived from the one-step global model and the temperature-dependent Arrhenius relation described in detail in the literature (Nyakuma, Wong, and Oladokun 2019). The OFW model equation is given as;

$$\ln(\beta) = \ln\left(\frac{k_o E_a}{Rg(\alpha)}\right) - 5.331 - 1.052\left(\frac{E_a}{RT}\right) \tag{1}$$

Based on Equation 1, $\ln(\beta)$ is plotted against $\left(\frac{1}{T}\right)$ to deduce the E_a (kJ/mol) and k_o (/min) for BNC from α = 0.5 to 0.95 during TGA. The terms β, R, and T denote the heating rate (K/min), molar gas constant (J/mol K); and temperature (K). Thus, the E_a and k_o were computed from the slope $-1.052\left(\frac{E_a}{R}\right)$ and intercept $\ln\left(\frac{k_o E_a}{R}\right)$, respectively.

Results and discussion

Isolated BNC product properties

The appearance of a white jelly sheet between the air and liquid layers of the HS broth indicated the effective production of BNC. The raw synthesized BNC initially appeared as brownish-yellow pellicles embedded with the components of the synthesis medium, as shown in Figure 1(a). The subsequent treatment and purification with a low concentration of sodium hydroxide (NaOH) turned the BNC pellicles into a brighter and transparent film, as shown in Figure 1(b). BNC is hydrogel in nature with 99% water content that comprises a cellulose-based network of microfibrils (Abba et al. 2017; Moon et al. 2011).

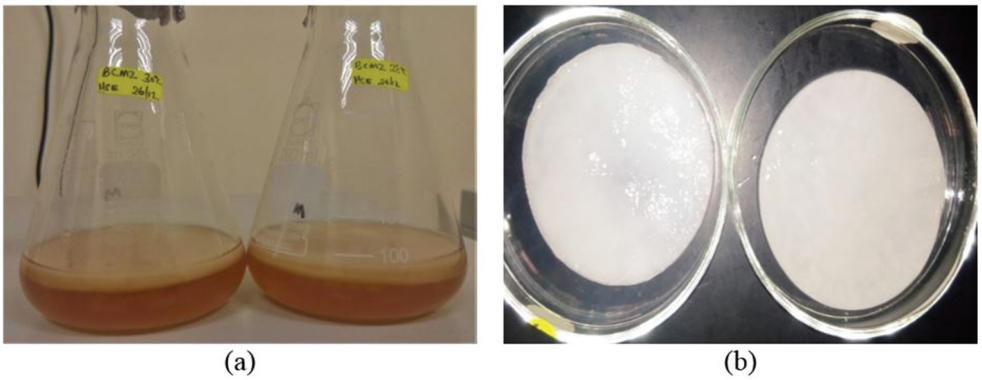

Figure 1. Synthesized BNC before treatment (a) after NaOH purification (b).

Morphological and bulk chemical properties

The morphology, microstructure, and bulk chemical composition of the *G. xylinus* synthesized BNC were examined by SEM and EDX techniques. The SEM micrograph of the BNC sample examined in this study is presented in Figure 2. The SEM micrograph revealed a rough surface and morphology characterized by highly dense fibrils and overlapping knots with asymmetric orientation. The unevenly dispersed fibrils and knots are interrupted by pores or spaces, which suggest a high surface area, roughness, porosity, and crystallinity (Mohammadkazemi et al. 2015). The roughness and porosity are typically ascribed to the selected techniques for treatment, purification or substrate employed in the isolation and synthesis of BNC. The selected techniques for producing BNC also influence the chemical composition of the final product. This observation is corroborated by Thorat and Dastager (2018) whose study showed marked differences in the BNC synthesized from glycerol (compact network and structure) and glucose (porous and reticular network structure). The bulk

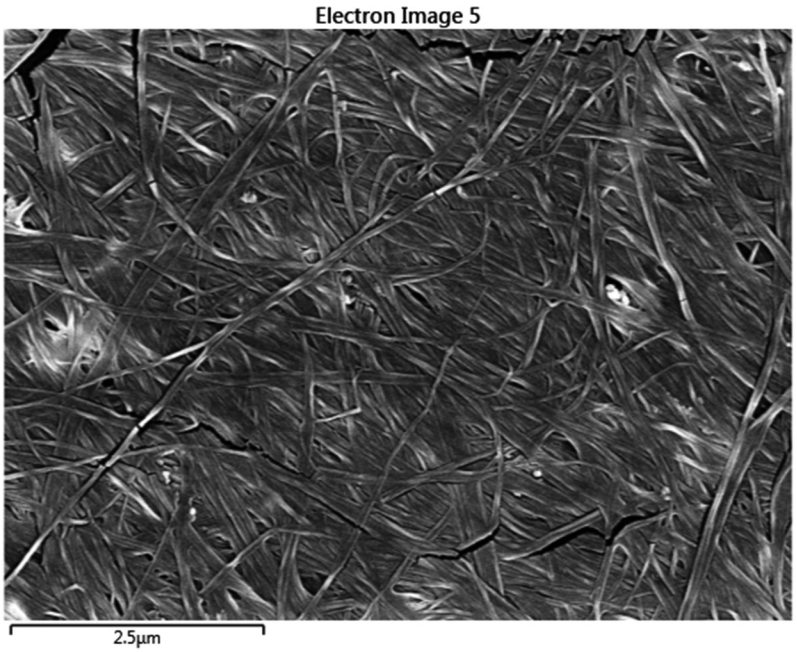

Figure 2. SEM micrograph of *G. xylinus* synthesized BNC at mag. ×1000.

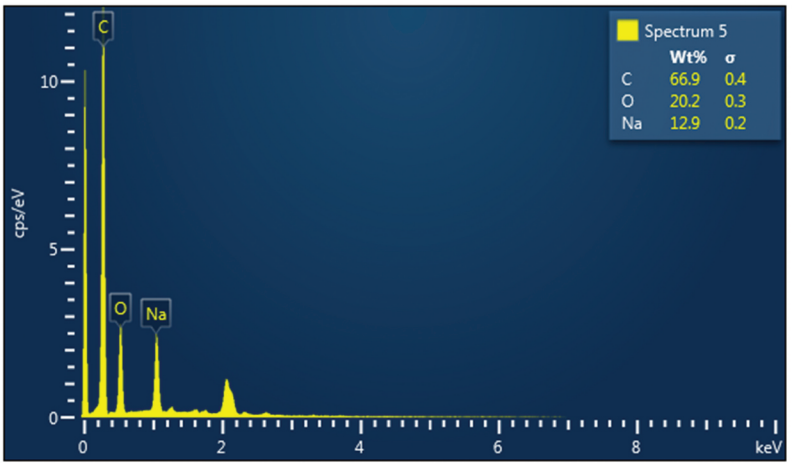

Figure 3. EDX spectrum of *G. xylinus* synthesized BNC at mag. ×1000.

chemical analysis of the BNC was examined through EDX analysis, as presented in the spectra in Figure 3. The bulk chemical properties of BNC determined by EDX analysis indicates that carbon (C), oxygen (O) and sodium (Na) are the primary elements in its chemical structure. The composition of the elements is in the order C > O > Na as shown in the EDX spectra. The high C and O content of BNC could be ascribed to cellulose, which has an empirical formula of $(C_6H_{10}O_5)_n$. In this study, the composition of C and O accounts for 87.1% of the overall elemental composition of BNC, which is in fairly good agreement with 93.83% computed for cellulose-based on its empirical formula. In contrast, the detection of Na in BNC during EDX is due to the alkali (NaOH) used to purify BNC post-synthesis and isolation. Similar findings are reported in the literature (Sakwises, Rodthongkum, and Ummartyotin 2017; Sanchis et al. 2017).

Thermal properties

Figure 4 presents the mass loss (TG, %) plots for the thermal degradation of *G. xylinus* synthesized BNC at multiple heating rates under the non-isothermal and non-oxidative conditions examined in this study. The TG plots reveal downward sloping curves from the left to the right-hand side of the graph indicating a significant loss of mass, typical of thermally degrading materials during TGA. The findings indicate that the stepwise increase in temperature from 28°C to 700°C resulted in the significant thermal degradation of BNC. Similarly, it was observed that TG plots shifted further to the right-hand side with increasing heating rates from 10°C/min to 50°C/min. These changes are ascribed to the thermal-time lag, which takes place when the heating rates are increased to higher values during TGA (Slopiecka, Bartocci, and Fantozzi 2012). Hence, the reaction time needed to attain equilibrium temperature by the thermally degrading materials is reduced, thereby causing the TG curves and their corresponding temperature profile characteristics (TPC) to shift to higher values. Table 1 presents the TPCs for BNC thermal degradation for each heating rate examined from the TG plots in this study. The findings reveal that the ignition (T_{ons}), midpoint (T_{mid}), burnout (T_{off}) temperatures of BNC all increased markedly with increasing heating rates during TGA. As can be observed in Table 1, the T_{ons} temperature increased by 25.14°C from 183.24°C to 208.38°C, whereas T_{mid} increased by 29.31°C from 269.30°C to 298.61°C, whereas T_{off} increased by 36.99°C from 363.79°C to 400.78°C. Hence, all the TPCs derived from the TG plots increased with increasing heating rates. Hence, the BNC degradation primarily occurred from 183.24°C to 400.78°C based on the minima and maxima of the T_{ons} and T_{off}, respectively, while the mean values of T_{ons}, T_{mid}, and T_{off} are 194.04°C, 283.69°C, and 384.15°C.

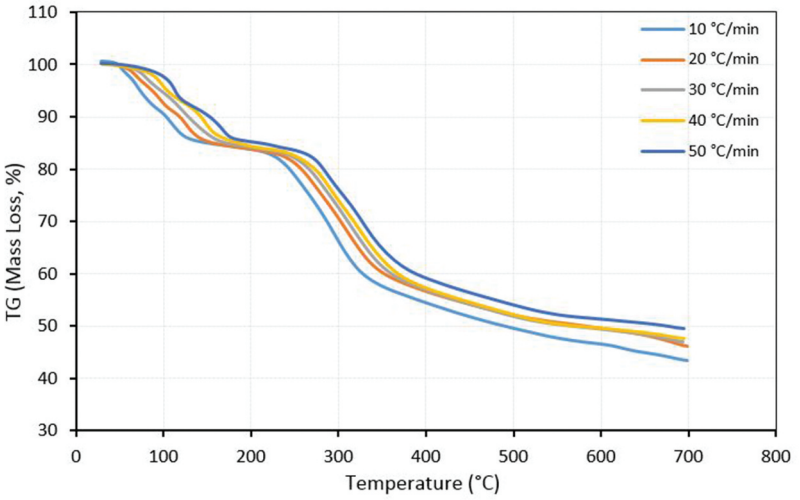

Figure 4. TG plots for thermal decomposition of BNC.

In comparison, the findings of Thorat and Dastager (2018) revealed T_{ons} and T_{off} values of 270°C and 395°C, whereas Niamsap, Lam, and Sukyai (2019) reported values between 292°C and 360°C, and Bhattacharya et al. (2020) revealed values of 250°C and 380°C for the thermal degradation of BNC, respectively. Hence, the results presented in this study are in good agreement with other reports in the literature. The mass loss (ML) and residual mass (RM) of BNC were also examined in this study. As observed in Table 1, the ML decreased from 57.24% to 50.74% (or 53.57% on average), whereas the RM showed an increasing trend from 42.76% to 49.26% (or 46.43% on average) with increasing heating rates during TGA. The trends observed for the ML and RM are ascribed to the effect of variable heating rates on thermal resistance and crystallinity of the nanosized BNC particles. Other factors such as the selected source of cellulose and pre-treatment methods also influence the thermal behavior of BNC (Santmartí and Lee 2018). Figure 5 shows the DTG plots for BNC thermal decomposition comprising several peaks of various sizes, shapes and symmetry during TGA. In general, the peaks broadly occurred in the ranges of (i) 28–200°C; (ii) 200–600°C; and (iii) 600–700°C.

The findings indicate that a series of complex and overlapping reactions also occurred during the multi-stage thermal degradation of BNC. The ML during the thermal degradation of BNC from 28°C to 200°C is characterized by a pair of small peaks typically ascribed to the loss of surface and inherent moisture (or drying) (Bhattacharya et al. 2020; Thorat and Dastager 2018). According to various authors (Molina-Ramírez et al. 2020; Ray and Cooney 2018), this drying stage is also termed the initiation stage of thermal degradation in the literature. The ML between 200°C and 600°C, also termed the prolongation stage (Molina-Ramírez et al. 2020; Ray and Cooney 2018), denotes the depolymerization, devolatilization, and degradation of cellulose and other volatile components (Thorat and Dastager 2018). However, Bhattacharya et al. (2020) attribute the ML to the mineralization of BNC in addition to

Table 1. Mass loss (TG, %) TPC values for BNC.

Heating rate (°C/min)	Onset (T_{ons}, °C)	Midpoint (T_{mid}, °C)	Burnout (T_{off}, °C)	Mass Lost (ML, %)	Residual Mass (RM, %)
10	183.24	269.30	363.79	57.24	42.76
20	188.11	272.47	370.05	54.21	45.79
30	194.35	285.00	386.32	53.21	46.79
40	196.12	293.09	399.80	52.46	47.54
50	208.38	298.61	400.78	50.74	49.26

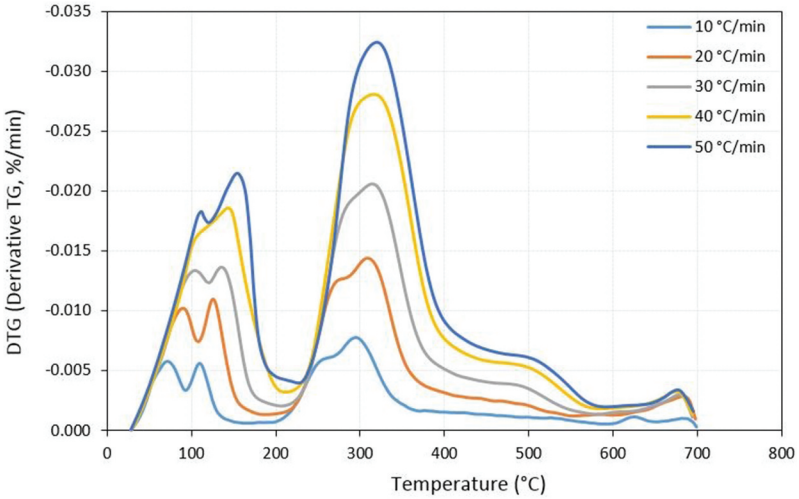

Figure 5. DTG plots for thermal decomposition of BNC.

cellulose depolymerization. The peaks in this stage are larger than the drying peaks and are characterized by the peak decomposition temperature denoted as T_{max} (see Table 2). The last stage or the termination step observed from 600°C to 700°C may be due to the degradation of pyrolytic char (Molina-Ramírez et al. 2020) formed by the depolymerization and devolatilization of cellulose during the TGA process.

Table 2 presents the TPC values for the derivative mass loss (DTG) plots for the thermal degradation of BNC. The TPCs comprise the drying peaks I and II ($T_{dry,\mathrm{I}}$ and $T_{dry,\mathrm{II}}$), maximum decomposition peak (T_{max}) temperature, and lastly mass-loss rates (MLR I, II) and MLR III for drying and devolatilization of BNC as deduced from Figure 5. The higher heating rates significantly influenced the TPCs and rate of mass loss during TGA. For all heating rates, the values of the drying peaks I and II ($T_{dry,\mathrm{I}}$ and $T_{dry,\mathrm{II}}$) and maximum decomposition peak (T_{max}) temperatures shifted to higher values as also observed for the TG plots. Hence, the average values for the TPCs at the drying peaks I and II ($T_{dry,\mathrm{I}}$ and $T_{dry,\mathrm{II}}$) are 112.67°C and 123.82°C, whereas the 311.50°C was computed for the maximum decomposition peak (T_{max}) temperatures. Conversely, the average mass loss rates are 3.90%/min (MLR I) and 2.55%/min (MLR II) for drying and 6.13%/min (MLR III) for the devolatilization of BNC. In comparison, the T_{max} for the BNC in this study ranged from 295.53°C to 323.18°C (or 311.50°C on average), which is lower than 361.50°C (Yingkamhaeng, Intapan, and Sukyai 2018), 395°C (Thorat and Dastager 2018), 348°C (Niamsap, Lam, and Sukyai 2019) and 353.30°C to 357.50°C (Molina-Ramírez et al. 2020) reported in the literature. The lower value of BNC in the current study may be due to the presence of Na as detected during EDX. The presence of metal elements typically catalyses the thermal degradation of bio-based materials. Besides, the TPCs and thermal degradation behavior of BNC are related to their physicochemical and mechanical attributes (e.g. surface area, density, and synthesis method) (Molina-Ramírez et al. 2020).

Table 2. Derivative mass loss (DTG, %/min) TPC values for BNC.

Heating rate (°C/min)	Drying Peak I (°C)	MLR I (%/min)	Drying Peak II (°C)	MLR II (%/min)	Decomp. Peak (T_{max}, °C)	MLR III (%/min)
10	71.95	1.21	109.32	1.32	295.53	2.50
20	91.34	2.74	126.21	2.08	307.92	4.25
30	103.23	3.52	135.94	4.26	314.46	6.00
40	141.95	5.44	145.67	6.44	316.42	8.04
50	154.88	6.57	154.50	8.62	323.18	9.86

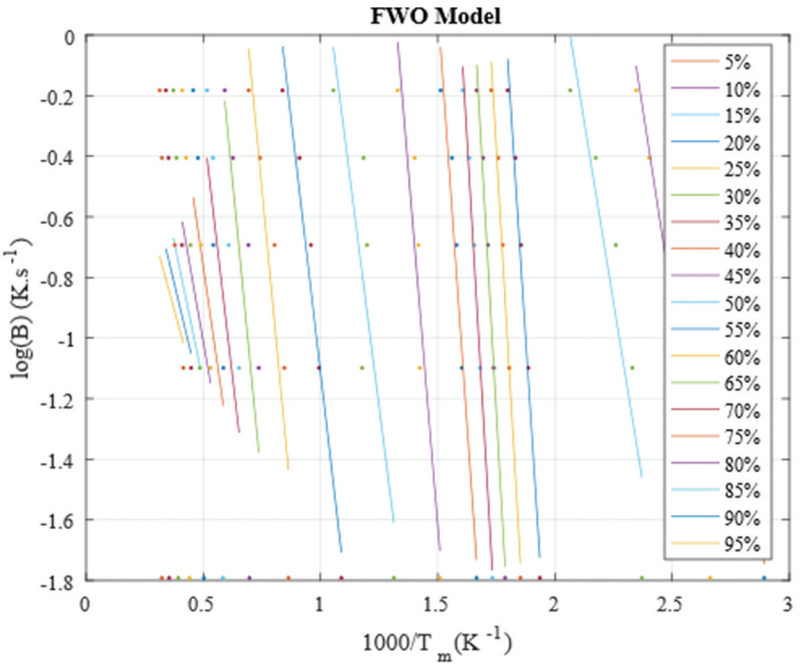

Figure 6. OFW plots for BNC kinetic degradation.

Kinetic properties

The activation energy (E_a) and pre-exponential factor (k_o) for BNC thermal degradation were computed from the plots of the Ozawa–Flynn–Wall (OFW) model presented in Figure 6. The OFW kinetic plots consist of various identically parallel plotted lines that indicate the BNC degradation process occurs through the first-order reaction. Typically, the order or arrangement of kinetic plots is critical for a comprehensive understanding of the process of biomass degradation (Abrishami et al. 2019) along with the reactivity, reaction pathway, and the potential yield and distribution of products (Nyakuma et al. 2015; Nyakuma, Wong, and Oladokun 2019). In this study, the kinetic parameters E_a and k_o were computed from the slope and intercepts of the kinetic plots of BNC degradation for conversions, α = 0.05–0.95 (or 5–95% conversions), as presented in Table 3. The findings showed that the kinetic parameters for the BNC degradation process ranged from 22.52 kJ/mol to 108.09 kJ/mol for activation energy (E_a), whereas k_o was between 8.99×10^{1} min^{-1} and 1.32×10^{11} min^{-1} resulting in the regression coefficient (R^2 = 0.0390–0.9925). The average values of the E_a = 59.39 kJ/mol, $k_o = 1.62 \times 10^{10}$ min^{-1} and R^2 = 0.66 indicate that BNC is highly thermally reactive compared to oil palm pellets (146.63 kJ/mol) (Nyakuma, Wong, and Oladokun 2019), corn stalk (206.40 kJ/mol), oak tree (236.20 kJ/mol), sawdust (232.60 kJ/mol) (Sun et al. 2006), cocoa shell (135.62 kJ/mol) (Mumbach et al. 2020), sugar cane bagasse (170.70 kJ/mol) (Da Silva et al. 2020).

Figure 7 presents the plot of the kinetic parameters (E_a and k_o) against the degree of conversion (α). As observed, the kinetic parameters fluctuated significantly during BNC degradation. Furthermore, the kinetic parameters versus degree of conversion plots reasonably confirm that the BNC degradation process occurs in three stages (I, II, and III), as earlier surmised. The values of kinetic parameters declined from α = 0.05 to 0.15, which denotes the first stage (I) i.e. drying or initiation of BNC as observed during TGA. Next, the parameters increased sharply from α = 0.15 to 0.50 with the maximum values of E_a and k_o observed at 108.09 kJ/mol and 1.13×10^{11} min^{-1}, respectively α = 0.30. These observations demarcate the second stage (II) or prolongation stage of the BNC

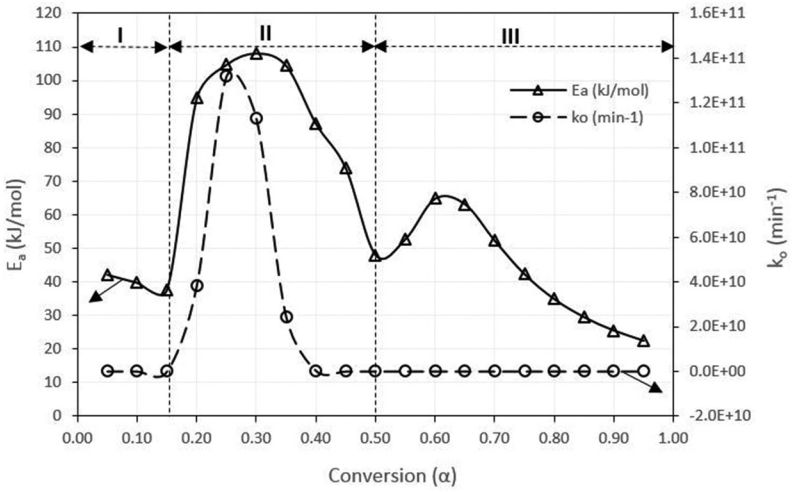

Figure 7. Kinetic parameter plots for BNC degradation.

Table 3. Computed kinetic parameters for BNC thermal degradation.

Conversion (a)	Coefficient of Regression (R^2)	Activation Energy (E_a, kJ/mol)	Pre-exponential factor (k_o, min^{-1})
0.05	0.9925	42.11	3.51×10^{7}
0.10	0.9740	39.75	5.19×10^{6}
0.15	0.8530	37.69	8.61×10^{5}
0.20	0.9840	94.75	3.84×10^{10}
0.25	0.9877	104.73	1.32×10^{11}
0.30	0.9899	108.09	1.13×10^{11}
0.35	0.9908	104.39	2.44×10^{10}
0.40	0.9595	87.14	3.28×10^{8}
0.45	0.8887	73.91	5.68×10^{6}
0.50	0.7686	48.04	2.09×10^{4}
0.55	0.9607	52.72	8.42×10^{3}
0.60	0.8440	64.82	7.47×10^{3}
0.65	0.5438	63.19	2.47×10^{3}
0.70	0.3171	52.32	6.63×10^{2}
0.75	0.1890	42.33	2.74×10^{2}
0.80	0.1188	34.90	1.62×10^{2}
0.85	0.0787	29.52	1.20×10^{2}
0.90	0.0544	25.55	9.99×10^{1}
0.95	0.0390	22.52	8.99×10^{1}
Average	***	59.39	1.62×10^{10}

degradation. Based on the maximal values observed, this stage is considered the slow or rate-determining stage, which is majorly characterized by the depolymerization and degradation of cellulose during TGA. The last stage (III) or termination was observed between α = 0.50 and 0.95 although the maximum E_a was observed at α = 0.6. Overall, the fluctuations confirm the BNC degradation process is a complex, multistep and first-order thermal process.

Potential applications of *G. xylinus* synthesized BNC

The synthesis of BNC from *G. xylinus* presents significant opportunities for application in various fields. The findings of this study indicate that the *G. xylinus* synthesized BNC has a high surface area, roughness, and porosity, which could be effectively applied in medical applications such as artificial

skins for the treatment of burns, ulcers, vascular grafts, dental implants, artificial blood vessels, and antimicrobial wound dressings as reported in the literature (Jozala et al. 2016; Shah et al. 2013a). Likewise, the 3D structural network of BNC has potential applications as natural scaffolds for tissue generation (Fu, Zhang, and Yang 2013a; Rajwade, Paknikar, and Kumbhar 2015). Other studies have also highlighted that BNC can be used to enhance drug delivery, protein loading and release, and oncological therapy (Müller et al. 2013; Numata, Mazzarino, and Borsali 2015). The myriad potentials of BNC for medical applications are due to its high elasticity, compatibility, transparency, and conformability. Furthermore, the high crystallinity presents opportunities for pharmaceutical applications such as the chemical conjugation and functional group modifications required for innovative loading and release of medicines (Akhlaghi, Berry, and Tam 2013; Jozala et al. 2016). Likewise, the detection of metal elements such as Na reported in this study, Cd (Bhattacharya et al. 2020), Fe nanoparticles (Yingkamhaeng, Intapan, and Sukyai 2018), together with Ca and P (Niamsap, Lam, and Sukyai 2019) indicates that in BNC can be tuned, functionalized, or impregnated for specialized applications. Alternatively, the high surface area and porosity of BNC could serve as absorbent or adsorbent materials for water or wastewater treatment, bioremediation, or the removal of heavy metals such as cadmium (Cd) and chromium (Cr) (Bhattacharya et al. 2020; Derami et al. 2019; Dong et al. 2019; Jahan, Kumar, and Verma 2018). The kinetic properties indicate that although BNC has low average activation energy (i.e. highly reactive), it is fairly thermally stable during degradation. Hence, BNC could be effectively applied in low-temperature cellulose applications.

Conclusions

The study presented novel findings on the comprehensive characterization of the morphological, thermal, and kinetic properties of *Gluconacetobacter xylinus* synthesized bacterial nanocellulose (BNC). Morphological analysis showed that BNC is characterized by high surface area, porosity and crystal structure, whereas the bulk chemical analysis revealed the presence of cellulose building block elements such as C and O, whereas Na metal was detected due to the alkali purification and treatment process. Thermal analysis under non-isothermal, multiple heating rates and non-oxidative conditions revealed BNC undergoes three-stage thermal degradation resulting in the mass loss (ML = 50.74% to 57.24%) and residual mass (RM = 42.76% to 49.26%). Kinetic analysis based on the isoconversional Ozawa–Flynn–Wall (OFW) model showed that BNC has low values of activation energies but high pre-exponential factors. Overall, the morphological, thermal, and kinetic properties of *G. xylinus* synthesized BNC highlight its potential for various medical, pharmaceutical, and materials applications.

Acknowledgments

The technical assistance of the Hydrogen and Fuel Cell Laboratory, Institute of Future Energy, and School of Chemical & Energy Engineering, and the University-Industry Research Laboratory, all at Universiti Teknologi Malaysia (Skudai Campus), are gratefully acknowledged.

ORCID

Bemgba B. Nyakuma http://orcid.org/0000-0001-5388-7950
Laura N. Utume http://orcid.org/0000-0002-9853-4806

References

Abba, M., B. B. Nyakuma, Z. Ibrahim, J. B. Ali, S. I. A. Razak, and R. Salihu. 2020. Physicochemical, Morphological, and Microstructural Characterisation of Bacterial Nanocellulose from *Gluconacetobacter xylinus BCZM*. *Journal of Natural Fibers* 1–12. doi:10.1080/15440478.2020.1857896.

Abba, M., M. Abdullahi, M. H. M. Nor, C. S. Chong, and Z. Ibrahim. 2017. Isolation and Characterisation of Locally Isolated *Gluconacetobacter xylinus BCZM sp*. with Nanocellulose Producing Potentials. *IET Nanobiotechnology* 12:52–56.

Abrishami, F., Chizari, M., Zohari, N. and Pourmosavi, S.A., 2019. Study on Thermal Stability and Decomposition Kinetics of Bis (2, 2-Dinitropropyl) Fumarate (BDNPF) as a Melt Cast Explosive by Model-Free Methods. Propellants, Explosives, Pyrotechnics, 44(11):1446–1449

Akhlaghi, S. P., R. C. Berry, and K. C. Tam. 2013. Surface Modification of Cellulose Nanocrystal with Chitosan Oligosaccharide for Drug Delivery Applications. *Cellulose* 20 (4):1747–64. doi:10.1007/s10570-013-9954-y.

Bhattacharya, A., Sadaf, A., Dubey, S., Singh, R.P. and Khare, S.K., 2020. Production and characterization of Komagataeibacter xylinus SGP8 nanocellulose and its calcite based composite for removal of Cd ions. Environmental Science and Pollution Research, 1–8. https://doi.org/10.1007/s11356-020-08845–7

Blanco, A., Monte, M.C., Campano, C., Balea, A., Merayo, N. and Negro, C., 2018. Nanocellulose for industrial use: cellulose nanofibers (CNF), cellulose nanocrystals (CNC), and bacterial cellulose (BC). In Handbook of Nanomaterials for Industrial Applications. 74–126, Elsevier BV, The Netherlands

Curvello, R., V. S. Raghuwanshi, and G. Garnier. 2019. Engineering Nanocellulose Hydrogels for Biomedical Applications. *Advances in Colloid and Interface Science* 267:47–61. doi:10.1016/j.cis.2019.03.002.

Da Silva, J. C. G., J. G. De Albuquerque, W. V. De Araujo Galdino, R. F. De Sena, and S. L. F. Andersen. 2020. Single-Step and Multi-Step Thermokinetic Study–Deconvolution Method as a Simple Pathway for Describe Properly the Biomass Pyrolysis for Energy Conversion. *Energy Conversion and Management* 209:112653. doi:10.1016/j.enconman.2020.112653.

Derami, H. G., Q. Jiang, D. Ghim, S. Cao, Y. J. Chandar, J. J. Morrissey, Y. S. Jun, and S. Singamaneni. 2019. A Robust and Scalable Polydopamine/Bacterial Nanocellulose Hybrid Membrane for Efficient Wastewater Treatment. *ACS Applied Nano Materials* 2 (2):1092–101. doi:10.1021/acsanm.9b00022.

Dong, X.-B., W. Huang, Y.-B. Bian, X. Feng, S. A. Ibrahim, D.-F. Shi, X. Qiao, and Y. Liu. 2019. Remediation and Mechanisms of Cadmium Biosorption by a Cadmium-Binding Protein from Lentinula edodes. *Journal of Agricultural and Food Chemistry* 67 (41):11373–79. doi:10.1021/acs.jafc.9b04741.

Dwivedi, K. K., Karmakar, M. and Chatterjee, P. 2020. Thermal Degradation, Characterization and Kinetic Modeling of Different Particle Size Coal through TGA. Thermal Science and Engineering Progress, 18, 100523

Fu, L., J. Zhang, and G. Yang. 2013a. Present Status and Applications of Bacterial Cellulose-Based Materials for Skin Tissue Repair. *Carbohydrate Polymers* 92 (2):1432–42. doi:10.1016/j.carbpol.2012.10.071.

Fu, L., P. Zhou, S. Zhang, and G. Yang. 2013b. Evaluation of Bacterial Nanocellulose-Based Uniform Wound Dressing for Large Area Skin Transplantation. *Materials Science and Engineering: C* 33 (5):2995–3000. doi:10.1016/j.msec.2013.03.026.

Gatenholm, P., and D. Klemm. 2010. Bacterial Nanocellulose as a Renewable Material for Biomedical Applications. *MRS Bulletin* 35 (3):208–13. doi:10.1557/mrs2010.653.

Hestrin, S., and M. Schramm. 1954. Synthesis of Cellulose by *Acetobacter xylinum*. 2. Preparation of Freeze-Dried Cells Capable of Polymerizing Glucose to Cellulose. *Biochemical Journal* 58 (2):345–52. doi:10.1042/bj0580345.

Jacek, P., F. Dourado, M. Gama, and S. Bielecki. 2019. Molecular Aspects of Bacterial Nanocellulose Biosynthesis. *Microbial Biotechnology* 12 (4):633–49. doi:10.1111/1751-7915.13386.

Jahan, K., N. Kumar, and V. Verma. 2018. Removal of Hexavalent Chromium from Potable Drinking Using a Polyaniline-Coated Bacterial Cellulose Mat. *Environmental Science: Water Research & Technology* 4:1589–603.

Jozala, A. F., L. C. De Lencastre-Novaes, A. M. Lopes, V. De Carvalho Santos-Ebinuma, P. G. Mazzola, A. Pessoa-Jr, D. Grotto, M. Gerenutti, and M. V. Chaud. 2016. Bacterial Nanocellulose Production and Application: A 10-Year Overview. *Appl Microbiol Biotechnol* 100 (5):2063–72. doi:10.1007/s00253-015-7243-4.

Kamel, R., N. A. El-Wakil, A. Dufresne, and N. A. Elkasabgy. 2020. Nanocellulose: From an Agricultural Waste to a Valuable Pharmaceutical Ingredient. *International Journal of Biological Macromolecules* 163:1579–90. doi:10.1016/j.ijbiomac.2020.07.242.

Kargarzadeh, H., I. Ahmad, I. Abdullah, A. Dufresne, S. Y. Zainudin, and R. M. Sheltami. 2012. Effects of Hydrolysis Conditions on the Morphology, Crystallinity, and Thermal Stability of Cellulose Nanocrystals Extracted from Kenaf Bast Fibers. *Cellulose* 19 (3):855–66. doi:10.1007/s10570-012-9684-6.

Klemm, D., D. Schumann, U. Udhardt, and S. Marsch. 2001. Bacterial Synthesized Cellulose—Artificial Blood Vessels for Microsurgery. *Progress in Polymer Science* 26 (9):1561–603. doi:10.1016/S0079-6700(01)00021-1.

Li, P., J. A. Sirviö, B. Asante, and H. Liimatainen. 2018. Recyclable Deep Eutectic Solvent for the Production of Cationic Nanocelluloses. *Carbohydrate Polymers* 199:219–27. doi:10.1016/j.carbpol.2018.07.024.

Lin, N., and A. Dufresne. 2014. Nanocellulose in Biomedicine: Current Status and Future Prospect. *European Polymer Journal* 59:302–25. doi:10.1016/j.eurpolymj.2014.07.025.

Martínez Ávila, H., S. Schwarz, E.-M. Feldmann, A. Mantas, A. Von Bomhard, P. Gatenholm, and N. Rotter. 2014. Biocompatibility Evaluation of Densified Bacterial Nanocellulose Hydrogel as an Implant Material for Auricular Cartilage Regeneration. *Applied Microbiology and Biotechnology* 98 (17):7423–35. doi:10.1007/s00253-014-5819-z.

Mohammadkazemi, F., K. Doosthoseini, E. Ganjian, and M. Azin. 2015. Manufacturing of Bacterial Nano-Cellulose Reinforced Fiber–Cement Composites. *Construction and Building Materials* 101:958–64. doi:10.1016/j.conbuildmat.2015.10.093.

Molina-Ramírez, C., A. Cañas-Gutiérrez, C. Castro, R. Zuluaga, and P. Gañán. 2020. Effect of Production Process Scale-up on the Characteristics and Properties of Bacterial Nanocellulose Obtained from Overripe Banana Culture Medium. *Carbohydrate Polymers* 240:116341. doi:10.1016/j.carbpol.2020.116341.

Moon, R. J., A. Martini, J. Nairn, J. Simonsen, and J. Youngblood. 2011. Cellulose Nanomaterials Review: Structure, Properties and Nanocomposites. *Chemical Society Reviews* 40:3941–94.

Müller, A., Z. Ni, N. Hessler, F. Wesarg, F. A. Müller, D. Kralisch, and D. Fischer. 2013. The Biopolymer Bacterial Nanocellulose as Drug Delivery System: Investigation of Drug Loading and Release Using the Model Protein Albumin. *Journal of Pharmaceutical Sciences* 102 (2):579–92. doi:10.1002/jps.23385.

Mumbach, G. D., Alves, J. L. F., Da Silva, J. C. G., Di Domenico, M., De Sena, R. F., Marangoni, C., Machado, R. a. F. and Bolzan, A. 2020. Pyrolysis of Cocoa Shell and Its Bioenergy Potential: Evaluating the Kinetic Triplet, Thermodynamic Parameters, and Evolved Gas Analysis Using TGA-FTIR. Biomass Conversion and Biorefinery 1–17. https://doi.org/10.1007/s13399-020-01058–5

Niamsap, T., N. T. Lam, and P. Sukyai. 2019. Production of Hydroxyapatite-Bacterial Nanocellulose Scaffold with Assist of Cellulose Nanocrystals. *Carbohydrate Polymers* 205:159–66. doi:10.1016/j.carbpol.2018.10.034.

Numata, Y., L. Mazzarino, and R. Borsali. 2015. A Slow-Release System of Bacterial Cellulose Gel and Nanoparticles for Hydrophobic Active Ingredients. *International Journal of Pharmaceutics* 486 (1–2):217–25. doi:10.1016/j.ijpharm.2015.03.068.

Nyakuma, B. B., A. Ahmad, A. Johari, T. A. Tuan, O. Oladokun, and D. Y. Aminu. 2015. Non-Isothermal Kinetic Analysis of Oil Palm Empty Fruit Bunch Pellets by Thermogravimetric Analysis. *Chemical Engineering Transactions* 45:1327–32.

Nyakuma, B. B., S. Wong, and O. Oladokun. 2019. Non-Oxidative Thermal Decomposition of Oil Palm Empty Fruit Bunch Pellets: Fuel Characterisation, Thermogravimetric, Kinetic, and Thermodynamic Analyses. *Biomass Conversion and Biorefinery*. doi:10.1007/s13399-019-00568-1.

Nyakuma, B. B., S. L. Wong, H. M. Faizal, H. U. Hambali, O. Oladokun, and T. A. T. Abdullah. 2020a. Carbon Dioxide Torrefaction of Oil Palm Empty Fruit Bunches Pellets: Characterisation and Optimisation by Response Surface Methodology. *Biomass Conversion and Biorefinery*. doi:10.1007/s13399-020-01071-8.

Nyakuma, B. B., S. L. Wong, O. Oladokun, A. A. Bello, H. U. Hambali, T. A. T. Abdullah, and K. Y. Wong. 2020b. Review of the Fuel Properties, Characterisation Techniques, and Pre-Treatment Technologies for Oil Palm Empty Fruit Bunches. *Biomass Conversion and Biorefinery*. doi:10.1007/s13399-020-01133-x.

Phanthong, P., G. Guan, Y. Ma, X. Hao, and A. Abudula. 2016. Effect of Ball Milling on the Production of Nanocellulose Using Mild Acid Hydrolysis Method. *Journal of the Taiwan Institute of Chemical Engineers* 60:617–22. doi:10.1016/j.jtice.2015.11.001.

Rajwade, J., K. Paknikar, and J. Kumbhar. 2015. Applications of Bacterial Cellulose and Its Composites in Biomedicine. *Applied Microbiology and Biotechnology* 99 (6):2491–511. doi:10.1007/s00253-015-6426-3.

Ray, S. and Cooney, R.P. 2018. Thermal degradation of polymer and polymer composites. In Handbook of environmental degradation of materials. 185–206. William Andrew Publishing, Elsevier BV, The Netherlands

Sakwises, L., N. Rodthongkum, and S. Ummartyotin. 2017. Sno2- and Bacterial-Cellulose Nanofiber-Based Composites as a Novel Platform for Nickel-Ion Detection. *Journal of Molecular Liquids* 248:246–52. doi:10.1016/j.molliq.2017.10.047.

Sanchis, M., M. Carsí, C. Gómez, M. Culebras, K. Gonzales, and F. Torres. 2017. Monitoring Molecular Dynamics of Bacterial Cellulose Composites Reinforced with Graphene Oxide by Carboxymethyl Cellulose Addition. *Carbohydrate Polymers* 157:353–60. doi:10.1016/j.carbpol.2016.10.001.

Santmartí, A. and Lee, K.-Y. 2018. Crystallinity and Thermal Stability of Nanocellulose. Nanocellulose and Sustainability: Production, properties, applications, and case studies, 67–86, CRC Press, Boca Raton, Florida, United States (US)

Shah, N., Ul-Islam, M., Khattak, W. A. and Park, J. K. 2013a. Overview of Bacterial Cellulose Composites: A Multipurpose Advanced Material. Carbohydrate Polymers 98(2): 1585–1598

Shankar, S., and J.-W. Rhim. 2016. Preparation of Nanocellulose from Micro-Crystalline Cellulose: The Effect on the Performance and Properties of Agar-Based Composite Films. *Carbohydrate Polymers* 135:18–26. doi:10.1016/j.carbpol.2015.08.082.

Skočaj, M. 2019. Bacterial Nanocellulose in Papermaking. *Cellulose* 26 (11):6477–88. doi:10.1007/s10570-019-02566-y.

Slopiecka, K., P. Bartocci, and F. Fantozzi. 2012. Thermogravimetric Analysis and Kinetic Study of Poplar Wood Pyrolysis. *Applied Energy* 97:491–97. doi:10.1016/j.apenergy.2011.12.056.

Soria-Verdugo, A., E. Goos, N. García-Hernando, and U. Riedel. 2018. Analyzing the Pyrolysis Kinetics of Several Microalgae Species by Various Differential and Integral Isoconversional Kinetic Methods and the Distributed Activation Energy Model. *Algal Research* 32:11–29. doi:10.1016/j.algal.2018.03.005.

Sun, Q., W. Li, H. Chen, B. Li, and Q. Sun. 2006. Devolatilization Characteristics of Shenmu Coal Macerals and Kinetic Analysis. *Energy Sources, Part A* 28 (9):865–74. doi:10.1080/009083190910361.

Thorat, M. N., and S. G. Dastager. 2018. High yield production of cellulose by a Komagataeibacter rhaeticus PG2 strain isolated from pomegranate as a new host. *RSC Advances* 8 (52):29797–805. doi:10.1039/C8RA05295F.

Yang, Y., J. Jia, J. Xing, J. Chen, and S. Lu. 2013. Isolation and Characteristics Analysis of a Novel High Bacterial Cellulose Producing Strain Gluconacetobacter Intermedius Cis26. *Carbohydrate Polymers* 92 (2):2012–17. doi:10.1016/j.carbpol.2012.11.065.

Yingkamhaeng, N., I. Intapan, and P. Sukyai. 2018. Fabrication and Characterisation of Functionalised Superparamagnetic Bacterial Nanocellulose Using Ultrasonic-Assisted in Situ Synthesis. *Fibers and Polymers* 19 (3):489–97. doi:10.1007/s12221-018-7738-6.

Zhuo, X., C. Liu, R. Pan, X. Dong, and Y. Li. 2017. Nanocellulose Mechanically Isolated from Amorpha fruticosa Linn. *ACS Sustainable Chemistry & Engineering* 5 (5):4414–20. doi:10.1021/acssuschemeng.7b00478.

View publication stats